Computational Investigation Of Nanofluid Heat Transfer Over A Stretched Sheet In The Presence Of A Magnetic Field

Sadia Irshad[1*], Shah Jahan[2], Afraz Hussain Majeed[3]

[1*]Institute of Mathematics, Khawaja Fareed University of Engineering and Information Technology, Rahim Yar Khan, Punjab 64200, Pakistan. Email: Sadiairshad15@gmail.com
[2]Institute of Mathematics, Khawaja Fareed University of Engineering and Information Technology, Rahim Yar Khan, Punjab 64200, Pakistan. Email: jahanshah@kfueit.edu.pk
[3]School of Energy and Power Engineering, Jiangsu University, Zhenjiang 212013, China. afraz@ujs.edu.cn

***Corresponding Author:** Sadia Irshad
*****Institute of Mathematics, Khawaja Fareed University of Engineering and Information Technology, Rahim Yar Khan, Punjab 64200, Pakistan. Email: sadiairshad15@gmail.com

Abstract
In this case, we look into remarkable effects of a magnetic field on flow, stagnation point as well as heat transfer phenomena induced by nanofluids in close proximity to a stretched sheet. Our investigation takes into consideration intricate interplay of Brownian motion and thermophoresis, adding an innovative dimension to the analysis. The temperature and nanoparticle concentration solutions are intimately tied to six key parameters, namely the velocity ratio (A), Lewis number (Le), Prandtl number ($\mathbf{Pr}$), Brownian motion (Nb) and the thermophoresis parameter (Nt). Employing the powerful technique of transformation based on similarities, we skillfully transform the complex nonlinear boundary layer equations into a set of connected higher-order ordinary differential equations, paving the way for deeper insights and meaningful advancements in the study of fluid dynamics and heat transfer. In this novel study, we numerically solve the equations to obtain velocity, temperature, and concentration distribution results. The skin friction coefficient, local Nusselt number, and Sherwood number are also calculated. Our findings indicate that as the velocity ratio parameter (A) increases, both skin friction coefficient (C_f) and local Nusselt number (Nu_x) rise. The local Sherwood number increases with higher A and Lewis number (Le). Additionally, we observe that when (A > 1), the heat transfer rate at the surface increases, and when (A< 1), it decreases. When compared to a previous study, there is excellent agreement.

Keywords: Stretching Sheet, Nanofluid, Magnetic field, Brownian motion, Thermophoresis.

1-Introduction:

Nanofluids represent a cutting-edge advancement in the heat transfer field, as they are meticulously engineered colloidal suspensions that incorporate nanoparticles within a base fluid. These nanoparticles, usually between 1 to 100 nanometers in size, are chosen for their exceptional thermal and physical attributes. The base fluid can be tailored to suit the application's requirements, with popular choices including water, ethylene glycol, and various oils. The unique combination of nanoparticles and base fluids grants nanofluids numerous advantages, making them increasingly prevalent across diverse industries and applications. A Computational Study holds significant significance as it delves into the promising research area heat transfer using nanofluids while considering magnetic field effect. Through the use of numerical simulations, the study explores velocity, temperature, and concentration distributions, along with essential parameters like skin friction coefficient (c_f) and Nusselt number (Nu_x). The findings help to a deeper understanding of nanofluid dynamics and magnetic field interactions, offering potential applications to optimize heat transfer in engineering processes and foster enhanced energy efficiency and sustainability. This knowledge can lead to improved heat transfer technologies and applications in various engineering fields.

The literature review by Choi [1]. extensively explores the current state and potential future research directions in nanofluid technology. Similarly, Yu et al. [2]. conducted a comprehensive review, focusing on nanofluid technology's applications in transportation and related fields. Li et al. [3]. examined the progress in nanofluid preparation and characterization, while Senthilraja et al. [4]. offered a comprehensive review of nanofluid applications in future autos, aiming to explore their potential uses and benefits in the automotive industry.

Suresh et al. [5]. conducted a research to examine the impact of Al_2O_3-Cu/water hybrid nanofluid on heat transfer. In a similar vein, Labib et al. [6]. carried out a numerical analysis to evaluate heat transfer characteristics of different base fluids and hybrid nanofluids under forced convection conditions. Madhesh et al. [7]. performed an experimental analysis to assess the thermal performance of a hybrid nanofluid as a cooling medium in comparison to conventional coolants. Their focus was on investigating the heat transfer characteristics and potential cooling efficiency enhancement.

Meanwhile, Esfe et al. [8]. conducted an empirical investigation to precisely determine a hybrid nanofluid's thermal conductivity and dynamic viscosity comprising Ag (silver) and MgO (magnesium oxide) nanoparticles in water. Their primary objective was to comprehensively analyze the heat transfer characteristics and flow behaviour of this nanofluid for potential applications in various heat transfer systems.

Das and his colleagues [9]. conducted an extensive review that centered on investigating thermal conductivity's influence and mechanism in both regular and hybrid nanofluids. Their study aimed to provide a detailed analysis of these fluids' thermal conductivity properties and explore the underlying mechanisms responsible for their heat transfer enhancements. In a separate study, Esfe et al. [10]. investigated SWCNT-MgO hybrid nanofluid thermal conductivity and performed some energy management price-performance analysis applications. Meanwhile, Huminic and his colleagues [11]. carried out a cutting-edge review of hybrid nanofluids for heat transfer applications. Their study aimed to offer a comprehensive overview of the current advancements and research progress in utilizing hybrid nanofluids for heat transfer purposes, covering various compositions, preparation methods, thermal conductivity enhancements, and potential applications. On a different note, Tlili et al. [12]. focused on macroscopic convection modelling in hybrid nanofluids with magnetic effects, aiming to understand the behavior of these nanofluids under magnetic fields' impact and their impact on convection. Lastly, Gul et al. [13]. investigated the effect of a magnetic dipole on the flow of hybrid nanofluids over an extending surface, aiming to gain insights into how the presence of a magnetic field influences the flow and heat transmission properties of these nanofluids.

In their study, Hussain and Jamshed [14]. conducted tangent hyperbolic hybrid nanofluid flow comparison entropy analysis, employing to investigate the flow, use the finite difference method characteristics of these nanofluids. In a separate investigation, Hussain and their colleague [15]. developed a computer model for investigating hybrid nanofluid flow on a spinning surface under convective conditions. On another front, Shoeibi et al. [16]. focused their study on the performance of a solar still employing hybrid nanofluid glass cooling. They integrated fluid dynamics computation simulations and environmental analysis to assess the efficiency of employing hybrid nanofluids with glass cooling in solar still systems. These research works contribute valuable insights into the behavior and applications of hybrid nanofluids, offering potential advancements in fluid dynamics and heat transfer studies.

The study conducted by Eid and Hossainy [17]. significantly contributes to the understanding of the hybrid nanofluid through a combined approach of experimental and computational techniques. Their findings provide valuable insights into the fluid dynamics, thermal properties, and potential applications of this nanofluid in diverse fields, including heat transfer systems and energy conversion devices. In a different study, Mandal et al. [18]. explore hybrid nanofluid magnetohydrodynamic (MHD) mixed convection in a novel W-shaped porous structure, uncovering key aspects of the nanofluid's behavior as a result of MHD and mixed convection in this specific configuration. Farooq et al. [19]. a radiative hybrid nanofluid over a stretched surface modelling and computational framework, emphasizing the effects of entropy generation and radiative heat transfer in this system. Additionally, Wanatasanappan and their colleague [20]. explore the viscosity and rheological properties of a hybrid nanofluid consisting of Al_2O_3- Fe_2O_3 nanoparticles distributed in a water-ethylene glycol combination, aiming to establish correlations between the nanofluid components and its viscosity properties. In another study, Zubair et al. [21]. compute the thermal conductivity of a radiative Williamson hybrid nanofluid, gaining valuable insights into the nanofluid's behavior concerning radiative heat transfer characteristics. Lastly, Sreedevi and Reddy [22]. conduct a research study on the flow behavior of Williamson hybrid nanofluid over a swirling cylinder, exploring the effects of Heat flow and gyrotactic microorganisms in the Cattaneo-Christov model in this specific flow scenario. These research efforts collectively advance the knowledge of the potential applications of hybrid nanofluids in different technical and industrial fields.

Yahya et al. [23]. conducted an investigation on the thermal properties of a Williamson hybrid nanofluid, including MoS2 and Zn O nanoparticles engine oil distributed, flowing over a stretched sheet. The researchers explored the Heat transport behaviour and thermal characteristics of this hybrid nanofluid in the presence of a sheet stretched. Alwawi et al. [24]. studied a Williamson hybrid nanofluid flowing over a cylindrical shape with magnetic and radiation effects' coupled convective energy transfer performance. In a separate study, Tawade et al. [25]. investigated the thermophoresis and Brownian motion effects on thermal and chemically reactive Casson nanofluid flow over a linearly stretched sheet. Reddy and his colleagues [26]. conducted a study to investigate the evaluating the implications of the Casson model on hybrid nanofluid flow over a moving thin needle of Dufour and Soret as well as thermal radiation. Meanwhile, Shah and Awan [27]. explored the over a three-dimensional (3D) sheet, analyzing the effects of magnetization, Darcy-Forchheimer layered rotating Williamson hybrid nanofluid flow's relevance model, and stratification on the flow behavior. Lastly, Jamshed et al. [28]. studied the entropy of a radiative Casson hybrid nanoliquid with variable thermal conductivity along a stretched surface. Their research aimed to analyze the entropy generation and thermal behavior of this hybrid nanoliquid under radiative heat transfer conditions using the Keller box method. These studies collectively advance the understanding of hybrid nanofluids and their thermal behavior, paving the way for potential applications in various engineering and industrial scenarios.

In their study, Alkasabeh [29]. investigated the numerical solution of a Casson hybrid nanofluid heat transfer flow over a vertical stretching sheet, taking into account the impact of a magnetic field. The research aimed to investigate the heat

transfer characteristics and flow of fluid behavior of the Casson hybrid nanofluid in the presence of a vertical stretching sheet and magnetic field. In a different numerical investigation, Paul et al. [30]. studied the transport of heat of a magnetohydrodynamic (MHD) Cu/Al_2O_3-H_2O Casson hybrid nanofluid flow through an exponentially extending cylinder with a heat source.

Moreover, Alkasasbeh et al. [31]. conducted research on the computer simulation of magneto convection flow of Williamson hybrid nanofluid, taking thermal radiation into account. Humane et al. [32]. conducted extensive research on the impact of the influence of chemical reaction and thermal radiation on the magnetohydrodynamic flow of Casson-Williamson nanofluid over a porous stretched surface has been studied. In a different study, Abbas et al. [33]. the effect of Ohmic dissipation on the flow of Casson-Williamson fluid across a slippery surface through a porous media was examined. Rashad et al. [34]. conducted a comprehensive study on the effect of heat variation on the magnetohydrodynamics (MHD) Williamson hybrid nanofluid flow in a porous medium with convective boundary conditions and Ohmic heating. Lastly, Divya et al. [35]. carried out an investigation on the unsteady magnetohydrodynamics (MHD) Casson and Williamson nanofluid flow through a permeable stretched sheet, considering the effects of thermal radiation and chemical reaction. These research studies add to our understanding of heat transfer and fluid flow behavior in various hybrid nanofluid systems, incorporating diverse parameters such as magnetic fields, thermal radiation, chemical reactions, and porous media.

This study aims to conduct a comprehensive computational investigation into the heat transfer properties of nanofluids flowing on top of a stretched sheet while considering the impact of an applied magnetic field. By employing computational simulations and modeling techniques, the research intends to gain valuable insights into the thermal behavior and fluid flow dynamics of these nanofluids under the effect of magnetic forces. The study's findings are intended to provide critical information for possible applications in various engineering and industrial scenarios, contributing to the advancement of more efficient and innovative heat transfer technologies.

2-Problem Formulation

In this particular investigation, we embark on exploring the intriguing behavior of a two-dimensional nanofluid stagnation point flow meets a stretched sheet. This nanofluid, a colloidal suspension created through engineering, incorporates suspended nanoparticles within a base liquid, resulting in remarkable enhancements in thermal and mechanical properties. The stretching sheet itself is meticulously maintained at specific constant values of temperature (T_w) and concentration (C_w), while the surrounding environment sets the backdrop with its ambient temperature (T_∞) and concentration (C_∞). Adding to the complexity of the scenario, a continuous transverse magnetic field of intensity is skillfully employed in the y-direction, perpendicular to the foreground. While acknowledging a small magnetic field, it is rightfully deemed negligible compared to the significant applied magnetics force. Furthermore, we consider an essential assumption that the thermal balance is maintained by the base fluid and nanoparticles, sharing a common temperature. Emphasizing the seamless movement, the fluid-nanoparticle interface adheres to a no-slip condition, ensuring coherent motion. Armed with this distinctive and comprehensive framework, we strive to unravel the intriguing dynamics of nanofluids as they interact with a stretched sheet enticingly influenced by an external magnetic field.

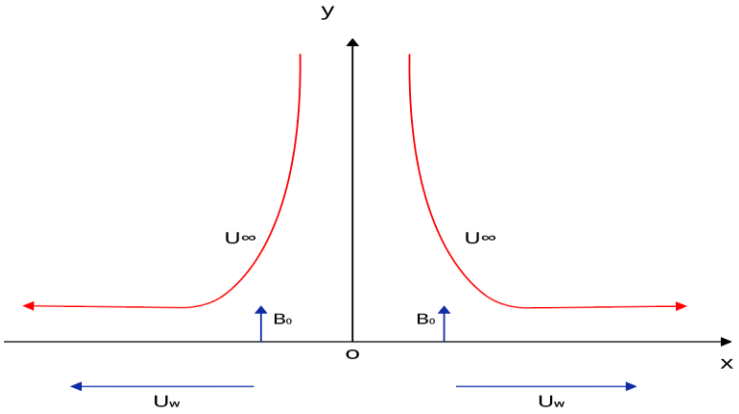

Figure 1. Geometry of flow of coordinate grid.

The governing equations for fluid dynamics and nanoparticle movement are the results of passing a stretched sheet in the presence of a magnetic field:

$$\frac{\partial u}{\partial x}+\frac{\partial v}{\partial y}=0 \qquad (1)$$

$$u\frac{\partial u}{\partial x}+v\frac{\partial u}{\partial y}=-\frac{1}{\rho_f}\frac{\partial p}{\partial x}+U_\infty\frac{\partial U_\infty}{\partial x}+\nu\left(\frac{\partial^2 u}{\partial x^2}+\frac{\partial^2 u}{\partial y^2}\right)+\frac{\sigma B_0^2}{\rho_f}\left(U_\infty-u\right) \quad (2)$$

$$u\frac{\partial v}{\partial x}+v\frac{\partial v}{\partial y}=-\frac{1}{\rho_f}\frac{\partial p}{\partial y}+\nu\left(\frac{\partial^2 v}{\partial x^2}+\frac{\partial^2 v}{\partial y^2}\right)+\frac{\sigma B_0^2}{\rho_f}v \quad (3)$$

$$u\frac{\partial T}{\partial x}+v\frac{\partial T}{\partial y}=\alpha\left(\frac{\partial^2 T}{\partial x^2}+\frac{\partial^2 T}{\partial y^2}\right)+\tau\left\{D_B\left(\frac{\partial\phi}{\partial x}\frac{\partial T}{\partial x}+\frac{\partial\phi}{\partial y}\frac{\partial T}{\partial y}\right)+\frac{D_T}{T_\infty}\left[\left(\frac{\partial T}{\partial x}\right)^2+\left(\frac{\partial T}{\partial y}\right)^2\right]\right\} \quad (4)$$

$$u\frac{\partial\phi}{\partial x}+v\frac{\partial\phi}{\partial y}=D_B\left(\frac{\partial^2\phi}{\partial x^2}+\frac{\partial^2\phi}{\partial y^2}\right)+\frac{D_T}{T_\infty}\left(\frac{\partial^2 T}{\partial x^2}+\frac{\partial^2 T}{\partial y^2}\right) \quad (5)$$

The boundary conditions are as follows:

$$u=u_w=ax, v=0, T=T_w, \phi=\phi_w \quad \text{at} \quad y=0$$

$$u\to U_\infty=bx, v=0, T\to T_\infty, \phi=\phi_\infty \quad \text{as} \quad y\to\infty. \quad (6)$$

The dimensionless quantities listed below are now introduced; the mathematical analysis of the problem is simplified by utilizing the similarity transforms described below:

$$\eta=\sqrt{\frac{a}{\nu}}y,\ \psi=\sqrt{a\nu x}\,f(\eta)$$

$$\theta(\eta)=\frac{T-T_\infty}{T_w-T_\infty},\ \phi(\eta)=\frac{\phi-\phi_\infty}{\phi_w-\phi_\infty} \quad (7)$$

The equation of continuity is satisfied if a stream function is chosen such that

$$u=\frac{\partial\psi}{\partial y}, \qquad v=-\frac{\partial\psi}{\partial x} \quad (8)$$

The governing equation is changed to the ordinary differential equation using the quantities of similarity transformation as follows:

$$f'''+ff''-f'^2+M(A-f')+A^2=0 \quad (9)$$

$$\theta''+\mathrm{Prf}\,\theta'+\mathrm{Pr}\,Nbh'\theta'+\mathrm{Pr}\,Nt\theta'^2=0 \quad (10)$$

$$h''+Lefh'+\frac{Nt}{Nb}\theta''=0 \quad (11)$$

In terms of boundary conditions

$$f(0)=0, f'(0)=1, \theta(0)=1, h(0)=1 \quad \text{at} \quad \eta=0,$$

$$f(\infty)=A, \theta(\infty)=0, \mathrm{h}(\infty)=0, \qquad \text{at} \quad \eta\to 0 \quad (12)$$

The following are the six controlling parameters:

$$A=\frac{b}{c},\ \mathrm{Pr}=\frac{\nu}{a},\ Le=\frac{\nu}{D_B},\ \mathrm{M}=\frac{\sigma B_0^2}{\rho_f c},\ \mathrm{Nb}=\frac{(\rho c)_p D_B(\phi_w-\phi_\infty)}{(\rho c)_f\nu},\ \mathrm{Nt}=\frac{(\rho c)_p D_B(T_w-T_\infty)}{(\rho c)_f\nu T_\infty}.$$

$$c_f=\frac{\tau_w}{\rho u_w^2},\ \mathrm{Nu}_x=\frac{xq_w}{k(T_w-T_\infty)},\ \mathrm{Sh}_x=\frac{xh_m}{D_B(\phi_w-\phi_\infty)}. \quad (13)$$

Where the wall's skin friction, heat flux, and mass flux are given by

$$\tau_w=\mu\left(\frac{\partial u}{\partial y}\right)_{y=0}, \mathrm{q}_w=-k\left(\frac{\partial T}{\partial y}\right)_{y=0}, \mathrm{h}_m=-D_B\left(\frac{\partial\phi}{\partial y}\right)_{y=0}.$$

Using the given equations, we obtain

$$c_f\sqrt{\mathrm{Re}_x} = f''(0), \frac{Nu_x}{\sqrt{\mathrm{Re}_x}} = -\theta'(0), \frac{Sh_x}{\sqrt{\mathrm{Re}_x}} = -h'(0). \quad (14)$$

Where are local Reynolds number Re_x, local Nusselt number Nu_x and local Sherwood number Sh_x, respectively.

Nomenclature

A	velocity ratio parameter
B_0	magnetic field strength
c_w	concentration at the surface of sheet
c_f	skin friction coefficient
c_∞	ambient concentration
f	dimensionless stream function
k	thermal conductivity
M	magnetic parameter
Nb	Brownian motion
Pr	Prandtl number
Le	Lewis number
T	Temperature of the fluid
Nu_x	local Nusselt number
Re_x	local Reynold number
Sh_x	local Sherwood number
Nt	thermophoresis parameter
T_w	temperature of the surface of the sheet
T_∞	Ambient temperature

3-Numerical Solution:

BVP4C (Boundary Value Problem with 4th Order Accuracy) can also be used to solve boundary value problems in magnetohydrodynamics (MHD). The system equations (9–11) can be solved by applying the boundary conditions (12) to bvp-4C. At first, BVP4C

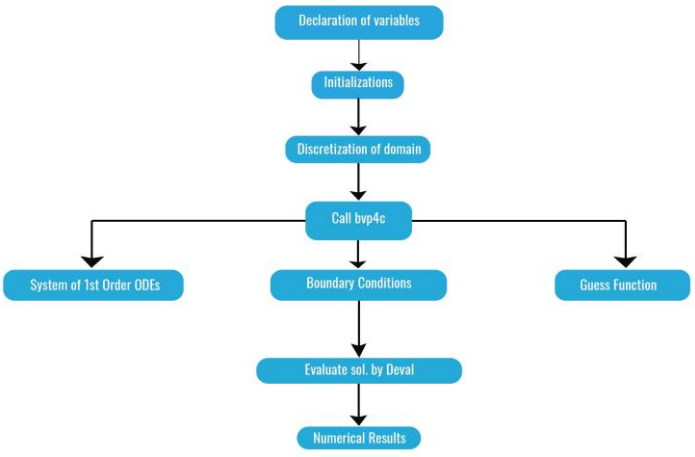

Figure 2. The bvp-4C method flow chart.

The equations (9-11) can be expressed as:

$$f''' = -ff'' + f'^2 - M(A - f') - A^2 \quad (15)$$

$$\theta'' = -\mathrm{Prf}\,\theta' - \mathrm{Pr}\,Nbh'\theta' - \mathrm{Pr}\,Nt\theta'^2 \quad (16)$$

$$h'' = -Lefh' - \frac{Nt}{Nb}\theta'' \quad (17)$$

The equation now defines new variables:

$$f = y(1), \mathrm{f}' = y(2), \mathrm{f}'' = y(3), \mathrm{f}''' = yy1, \theta = y(4), \theta' = y(5), \theta'' = yy2, \mathrm{h} = y(6), \mathrm{h}' = y(7), \mathrm{h}'' = \mathrm{yy}3.$$

The boundary condition and the three connected higher order differential equations can be transformed:

$$yy1 = -y(1)y(3) + y(2)^2 - M\left(A - y(2)\right) - A^2 \quad (18)$$

$$yy2 = -\Pr\, y(1)\, y(5) - \Pr\, Nby(7)\, y(5) - \Pr\, Nty(5)^2 \quad (19)$$

$$\mathrm{yy}3 = -Ley(1)\, y(7) - \frac{Nt}{Nb}\, yy2 \quad (20)$$

The border condition is transformed into

$$y(1) = 0, y(2) = 1, \mathrm{y}(4) = 1, \mathrm{y}(6) = 1 \text{ at } \eta = 0$$

$$y(2) = A, \theta(4) = 0, \mathrm{h}(6) = 0 \quad \text{as} \quad \eta \to \infty. \quad (21)$$

4-Result and Discussions:

The modified equations describing momentum, energy, and concentration (Equations 9-10) under the influence of the specified boundary conditions (Equation 11) were effectively solved using the BVP4C numerical method coupled with a shooting technique. By employing this approach, we successfully generated graphical representations of the velocity, temperature, and concentration profiles for a range of distinct governing parameter values. The outcomes of our analysis are visually presented in Figures (3-5) velocity, (6-8) temperature and (9-11) concentration.

The velocity graphs in Figures (3-5) demonstrate variations in the velocity ratio (A) and magnetic parameter (M) while maintaining other parameters constant. In particular, Figure (3) emphasizes how the velocity ratio parameter (A) affects the velocity graph. The flow velocity increases when the free stream velocity rises above the stretching sheet velocity, and at the same time, the thickness of the boundary layer decreases (A). The flow velocity and boundary layer thickness, on the other hand, both fall when the free stream velocity is smaller than the stretching velocity. When (A), the flow displays a boundary layer structure with a decreasing boundary layer thickness as (A) rises. While an inverted boundary layer structure appears for (A1), on the other hand. The thickness of the boundary layer also reduces in this case as the value of A does.

The significance of the magnetic field's influence on the flow characteristics is indicated by the magnetic parameter (M). A Lorentz force is introduced by the presence of a transverse magnetic field, and this force causes the velocity field to be retarded. As a result, the retarding force becomes stronger with larger values of (M), which causes a decrease in velocity. Figure (4) depicts this behaviour. When A=3.3, which denotes that (b/a=1), the flow displays a boundary layer structure. The boundary layer thickness within this framework decreases as the (M) values rise, illuminating a clear trend.

The flow field velocity variations related to the magnetic field and velocity ratio A are shown in Figure (5). In this investigation, we look at three different A values: A = 3.3, A = 1.0, and A = 0.2. When A=3.3, indicating that (b/a>1), a boundary layer structure is seen in the flow. According to this model, the magnetic field value M causes a decrease in the boundary layer's thickness. The velocity profiles for various M values coincide at A=1.0, showing that the magnetic field has little effect on the velocity graph in these circumstances. When (A<1) is present, on the other hand, an inverted boundary layer structure appears. This behaviour results from the fact that the stretching velocity ax of the surface exceeds the free stream velocity bx in these circumstances. The boundary layer thickness decreases with increasing M even in this circumstance. This result points to an increase in surface velocity gradient magnitude.

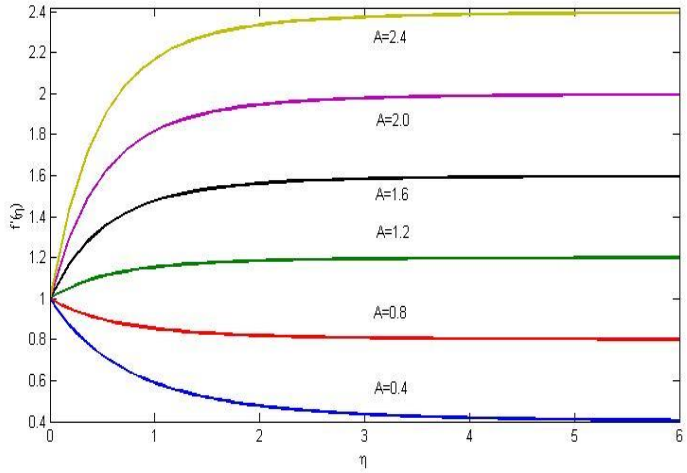

Figure 3. Velocity profile for various A values.

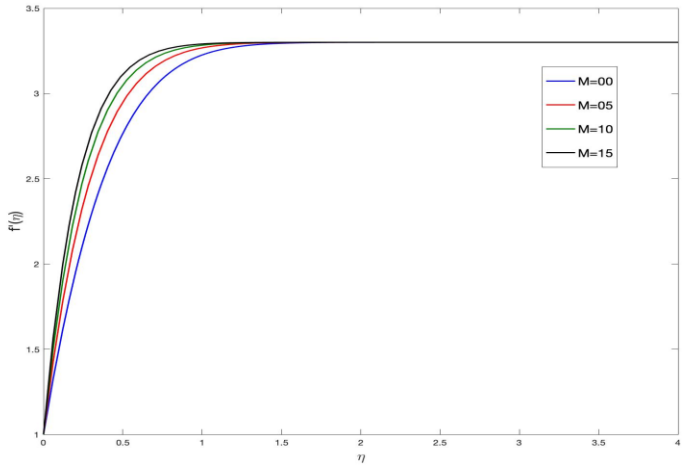

Figure 4. Velocity profile for various M values.

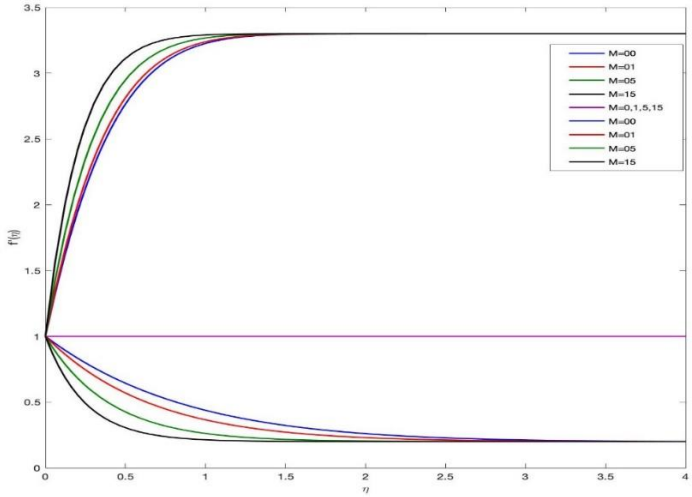

Figure 5. Velocity profile for various A & M values.

Figure (6) presents a comprehensive illustration of how alterations in the Brownian motion parameter and the thermophoresis parameter distinctly impact the temperature profile. An intriguing observation emerges: elevating the thermophoresis parameter prompts a proportional expansion in the thickness of the thermal boundary layer. This expansion is accompanied by a concurrent decrement in the difference in surface temperature, an effect attributed to the simultaneous elevation of both Nb and Nt. As a consequence of these interactions, the local Nusselt number, which serves as a reliable gauge of surface heat transfer efficiency, exhibits a consistent and noticeable decline.

Figure (7) illustrates the response of the temperature profile to variations in the velocity ratio parameter A. Notably, as the A parameter increases, there is a distinct decrease in the thickness of the thermal boundary layer. Furthermore, the surface temperature gradient experiences an upward trend in direct correlation with the increasing values of A.

Figure (8) portrays the temperature graph's variation concerning changes in the Prandtl number. The visualization highlights a noteworthy pattern: an escalation in the Prandtl number prompts a corresponding decrease in temperature, while keeping eta values constant. This trend stems from the intrinsic characteristics of higher Prandtl number fluids, which exhibit relatively lower thermal conductivity. Consequently, this reduction in thermal conductivity leads to a diminished conduction effect, resulting in a thinner thermal boundary layer and subsequently causing a decrease in temperature. Notably, the parallels between the impact of Prandtl number on Newtonian fluids and nanofluids are evident, signifying the inheritance of these properties in the nanofluid context as well.

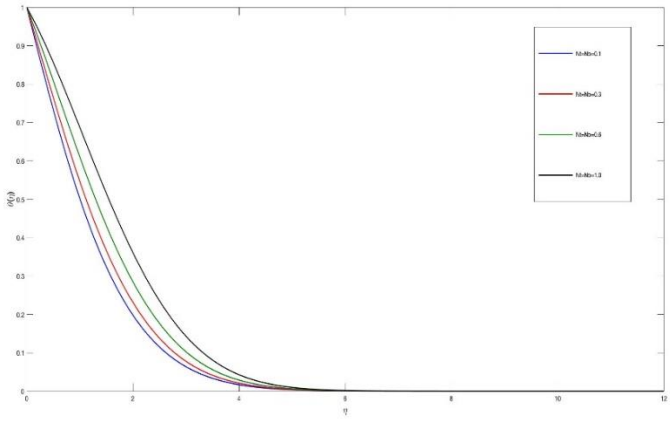

Figure 6. Temperature profile for various $Nt = Nb$ values.

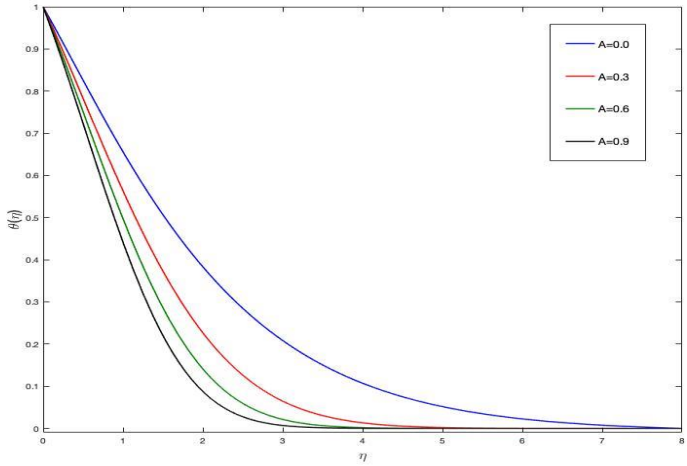

Figure 7. Temperature profile for various A values.

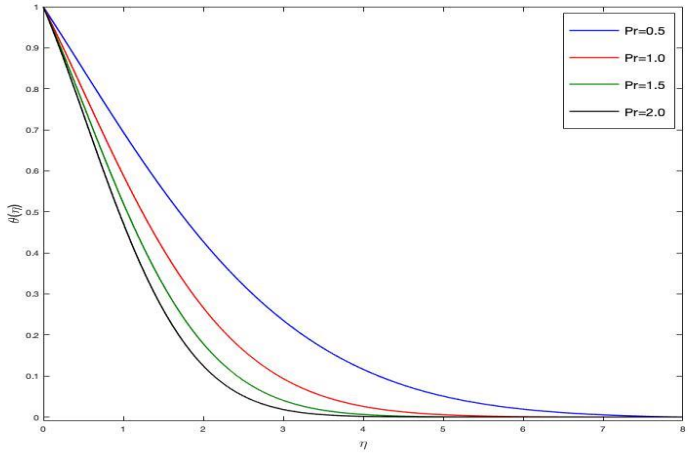

Figure 8. Temperature profile for various Pr values.

Figures (9-11) visually capture the alterations in nanoparticle concentration, correlating them to shifts in key governing parameters. These parameters encompass the velocity ratio, Brownian motion parameters, thermophoresis parameter, and Lewis number, collectively showcasing the dynamic interplay between these factors and nanoparticle concentration.

Figure (9) illustrates the velocity ratio parameter's impact on the concentration graph. A clear trend emerges: as the values of A increase, the concentration boundary layer's thickness has clearly decreased. Furthermore, the graph unmistakably portrays that the surface temperature gradient's magnitude intensifies in direct correlation with the escalating A values.

In Graph (10), a notable observation arises: an improvement in the Lewis number represents a decline in the concentration graph. This change is accompanied by a reduction in the thickness of the concentration boundary layer, a phenomenon

likely attributed to the heightened mass transfer rate as the Lewis number grows. Additionally, the graph shows an enhanced concentration gradient at the plate's surface.

Turning to Graph (11), it unveils the response of the concentration graph to fluctuations in the Brownian motion parameter. Remarkably, with an elevation in the values of the Brownian motion parameter, a discernible pattern emerges: the thickness of the concentration boundary layer exhibits a decrease. Strikingly, the graph also signifies that variations in the Brownian motion parameter have minimal impact on the thermal boundary layer thickness when Nb values are increased.

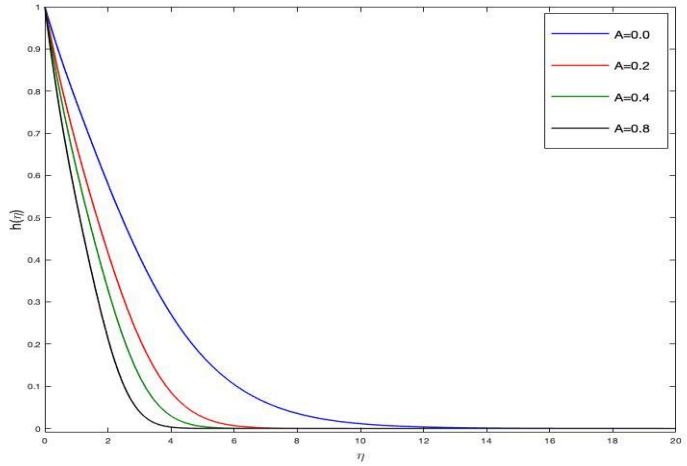

Figure 9. Concentration profile for various A values.

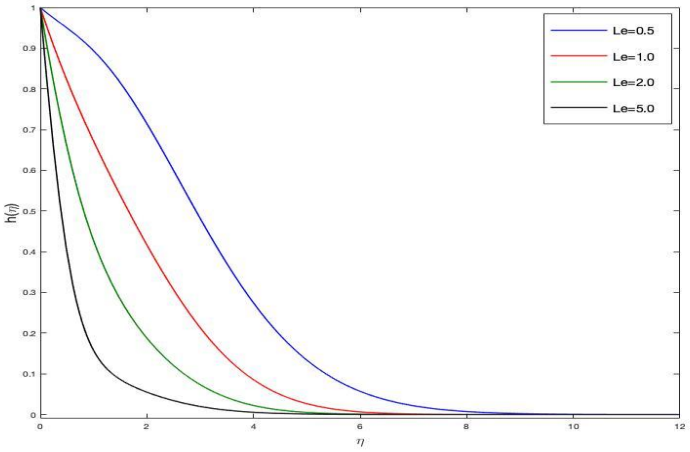

Figure 10. Concentration profile for various Le values.

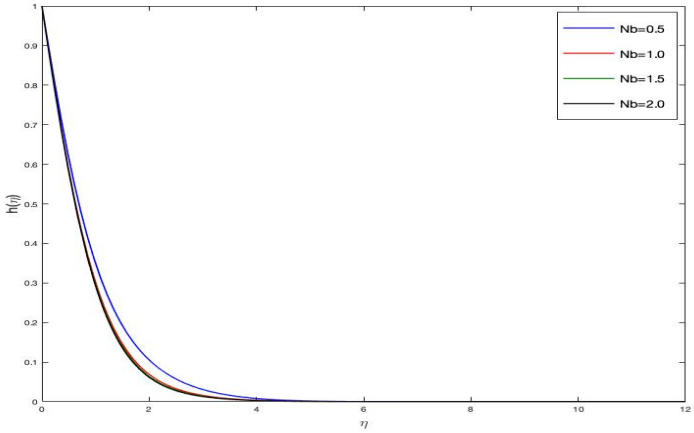

Figure 11. Concentration profile for various Nb values.

Table 1.

When $M = 0$, the values of $f''(0)$ are compared to the prior result.

A	Present result	Hayat [36]	Mahapatra [37]
0.01	-0.9981	-0.99823	-
0.10	-0.9693	-0.96954	-0.9694
0.20	-0.9183	-0.91813	-0.9181
0.50	-0.6674	-0.66735	-0.6673
2.00	2.0174	2.01767	2.0175
3.00	4.7292	4.72964	4.7292

Table 2. Comparison of the local Nusselt number $-\theta'(0)$ at $Nt = Nb = 0$ for various Pr values with previously reported data.

Pr	A	Present work	Hayat [36]	Mahapatra [37]
1	0.10	0.60221	0.602156	0.603
-	0.20	0.62452	0.624467	0.625
-	0.50	0.69242	0.692460	0.692
1.5	0.10	0.77681	0.776802	0.777
-	0.20	0.77712	0.797122	0.797
-	0.50	0.86343	0.864771	0.863

Table 1 makes it evident that there is great agreement between the results from [36] and [37] and the numerical values of the skin friction coefficient in this work for various values of A, when M=0. To further validate the research technique, Table 2 compares the local Nusselt number for various values of the velocity ratio parameter A with the Prandtl number Pr while ignoring the effects of M,Nb, and Nt parameters.

Nanoparticles are suspended in a base fluid to improve its thermal conductivity in nanofluid heat and mass transfer. This is useful for a variety of sectors, including electronics cooling, heat exchangers, solar thermal systems, and biological therapies including hyperthermia and tailored medication administration. It's essential for boosting innovation in various areas and for enhancing energy efficiency, lowering environmental impact, and minimizing it.

Conclusions

We have undertaken a novel theoretical exploration concerning the influences of distinct governing parameters. These parameters include the "M" magnetic parameter, the "A" velocity ratio parameter, the "Pr" Prandtl number, the "Nb" Brownian motion parameter, the "Nt" thermophoresis parameter, and the "Le" Lewis number. In the context of an MHD stagnation point flow of a nanofluid directed at a stretching sheet, our research focuses on closely analysing how these factors interact to alter the flow field and heat transfer properties.

The outcomes derived from our numerical analysis showcase a striking concurrence with data that has been previously documented within the academic literature. This notable agreement is especially pronounced within specific limits that correspond to particular cases elucidated in our ongoing study.

Here are the summarized conclusions drawn from the analysis:

- The velocity profile graph shows an increase when the velocity ratio parameter A>1.
- The thickness of the velocity boundary layer decreases as the magnetic field value M is increased.
- The reduction in the thickness of the thermal boundary layer is influenced by both the velocity ratio parameter A and the Prandtl number Pr.
- As the $Nt = Nb$ parameter increases, the thermal boundary layer's thickness grows as well.
- An increase in the wall temperature gradient is correlated with an increase in the Lewis number Le and the Prandtl number Pr.

References:

1. Choi, S. U. S. (1998). Nanofluid technology: current status and future research (No. ANL/ET/CP-97466). Argonne National Lab.(ANL), Argonne, IL (United States).
2. Yu, W., France, D. M., Choi, S. U., & Routbort, J. L. (2007). Review and assessment of nanofluid technology for transportation and other applications (No. ANL/ESD/07-9). Argonne National Lab.(ANL), Argonne, IL (United States).
3. Li, Y., Tung, S., Schneider, E., & Xi, S. (2009). A review on development of nanofluid preparation and characterization. Powder technology, 196(2), 89-101.
4. Senthilraja, S., Karthikeyan, M., & Gangadevi, R. (2010). Nanofluid applications in future automobiles: comprehensive review of existing data. Nano-Micro Letters, 2, 306-310.
5. Suresh, S., Venkitaraj, K. P., Selvakumar, P., & Chandrasekar, M. (2012). Effect of Al2O3–Cu/water hybrid nanofluid in heat transfer. Experimental Thermal and Fluid Science, 38, 54-60.
6. Labib, M. N., Nine, M. J., Afrianto, H., Chung, H., & Jeong, H. (2013). Numerical investigation on effect of base fluids and hybrid nanofluid in forced convective heat transfer. International Journal of Thermal Sciences, 71, 163-171.
7. Madhesh, D., & Kalaiselvam, S. (2014). Experimental analysis of hybrid nanofluid as a coolant. Procedia engineering, 97, 1667-1675.

8. Esfe, M. H., Arani, A. A. A., Rezaie, M., Yan, W. M., & Karimipour, A. (2015). Experimental determination of thermal conductivity and dynamic viscosity of Ag–MgO/water hybrid nanofluid. International Communications in Heat and Mass Transfer, 66, 189-195.
9. Das, P. K. (2017). A review based on the effect and mechanism of thermal conductivity of normal nanofluids and hybrid nanofluids. Journal of Molecular Liquids, 240, 420-446.
10. Esfe, M. H., Alirezaie, A., & Rejvani, M. (2017). An applicable study on the thermal conductivity of SWCNT-MgO hybrid nanofluid and price-performance analysis for energy management. Applied Thermal Engineering, 111, 1202-1210.
11. Huminic, G., & Huminic, A. (2018). Hybrid nanofluids for heat transfer applications–a state-of-the-art review. International Journal of Heat and Mass Transfer, 125, 82-103.
12. Tlili, I., Bhatti, M. M., Hamad, S. M., Barzinjy, A. A., Sheikholeslami, M., & Shafee, A. (2019). Macroscopic modeling for convection of Hybrid nanofluid with magnetic effects. Physica A: Statistical Mechanics and its Applications, 534, 122136.
13. Gul, T., Khan, A., Bilal, M., Alreshidi, N. A., Mukhtar, S., Shah, Z., & Kumam, P. (2020). Magnetic dipole impact on the hybrid nanofluid flow over an extending surface. Scientific Reports, 10(1), 1-13.
14. Hussain, S. M., & Jamshed, W. (2021). A comparative entropy based analysis of tangent hyperbolic hybrid nanofluid flow: Implementing finite difference method. International Communications in Heat and Mass Transfer, 129, 105671.
15. Hussain, A., Alshbool, M. H., Abdussattar, A., Rehman, A., Ahmad, H., Nofal, T. A., & Khan, M. R. (2021). A computational model for hybrid nanofluid flow on a rotating surface in the existence of convective condition. Case Studies in Thermal Engineering, 26, 101089.
16. Shoeibi, S., Kargarsharifabad, H., Rahbar, N., Ahmadi, G., & Safaei, M. R. (2022). Performance evaluation of a solar still using hybrid nanofluid glass cooling-CFD simulation and environmental analysis. Sustainable Energy Technologies and Assessments, 49, 101728.
17. Eid, M. R., & Al-Hossainy, A. F. (2023). Combined experimental thin film, DFT-TDDFT computational study, flow and heat transfer in [PG-MoS2/ZrO2] C hybrid nanofluid. Waves in Random and Complex Media, 33(1), 1-26.
18. Mandal, D. K., Biswas, N., Manna, N. K., Gorla, R. S. R., & Chamkha, A. J. (2023). Hybrid nanofluid magnetohydrodynamic mixed convection in a novel W-shaped porous system. International Journal of Numerical Methods for Heat & Fluid Flow, 33(2), 510-544.
19. Farooq, U., Waqas, H., Aldhabani, M. S., Fatima, N., Alhushaybari, A., Ali, M. R., ... & Muhammad, T. (2023). Modeling and computational framework of radiative hybrid nanofluid configured by a stretching surface subject to entropy generation: Using Keller box scheme. Arabian Journal of Chemistry, 16(4), 104628.
20. Wanatasanappan, V. V., Kanti, P. K., Sharma, P., Husna, N., & Abdullah, M. Z. (2023). Viscosity and rheological behavior of Al2O3-Fe2O3/water-EG based hybrid nanofluid: A new correlation based on mixture ratio. Journal of Molecular Liquids, 375, 121365.
21. Zubair, T., Usman, M., Hamid, M., Sohail, M., Nazir, U., Nisar, K. S., & Vijayakumar, V. (2021). Computational analysis of radiative Williamson hybrid nanofluid comprising variable thermal conductivity. Japanese Journal of Applied Physics, 60(8), 087004.
22. Sreedevi, P., & Reddy, P. S. (2021). Williamson hybrid nanofluid flow over swirling cylinder with Cattaneo–Christov heat flux and gyrotactic microorganism. Waves in Random and Complex Media, 1-28.
23. Yahya, A. U., Salamat, N., Huang, W. H., Siddique, I., Abdal, S., & Hussain, S. (2021). Thermal charactristics for the flow of Williamson hybrid nanofluid (MoS2+ ZnO) based with engine oil over a streched sheet. Case Studies in Thermal Engineering, 26, 101196.
24. Alwawi, F. A., Al Faqih, F. M., Swalmeh, M. Z., & Ibrahim, M. A. H. (2022). Combined convective energy transmission performance of Williamson hybrid nanofluid over a cylindrical shape with magnetic and radiation impressions. Mathematics, 10(17), 3191.
25. Tawade, J. V., Guled, C. N., Noeiaghdam, S., Fernandez-Gamiz, U., Govindan, V., & Balamuralitharan, S. (2022). Effects of thermophoresis and Brownian motion for thermal and chemically reacting Casson nanofluid flow over a linearly stretching sheet. Results in Engineering, 15, 100448.
26. Reddy, V. S., Kandasamy, J., & Sivanandam, S. (2022). Impacts of Casson Model on Hybrid Nanofluid Flow over a Moving Thin Needle with Dufour and Soret and Thermal Radiation Effects. Mathematical and Computational Applications, 28(1), 2.
27. Shah, S. A. A., & Awan, A. U. (2022). Significance of magnetized Darcy-Forchheimer stratified rotating Williamson hybrid nanofluid flow: A case of 3D sheet. International Communications in Heat and Mass Transfer, 136, 106214.
28. Jamshed, W., Mohd Nasir, N. A. A., Brahmia, A., Nisar, K. S., & Eid, M. R. (2022). Entropy analysis of radiative [MgZn6Zr-Cu/EO] Casson hybrid nanoliquid with variant thermal conductivity along a stretching surface: Implementing Keller box method. Proceedings of the Institution of Mechanical Engineers, Part C: Journal of Mechanical Engineering Science, 236(12), 6501-6520.
29. Alkasasbeh, H. (2022). Numerical solution of heat transfer flow of casson hybrid nanofluid over vertical stretching sheet with magnetic field effect. CFD Letters, 14(3), 39-52.
30. [30]- Paul, A., Das, T. K., & Nath, J. M. (2022). Numerical investigation on the thermal transportation of MHD Cu/Al 2 O 3-H 2 O Casson-hybrid-nanofluid flow across an exponentially stretching cylinder incorporating heat source. Physica Scripta, 97(8), 085701.

31. Alkasasbeh, H., Al Faqih, F. M., & Shoul, A. S. (2023). Computational Simulation of Magneto Convection Flow of Williamson Hybrid Nanofluid with Thermal Radiation Effect. CFD Letters, 15(4), 92-105.
32. Humane, P. P., Patil, V. S., & Patil, A. B. (2021). Chemical reaction and thermal radiation effects on magnetohydrodynamics flow of Casson–Williamson nanofluid over a porous stretching surface. Proceedings of the Institution of Mechanical Engineers, Part E: Journal of Process Mechanical Engineering, 235(6), 2008-2018.
33. Abbas, W., Megahed, A. M., Ibrahim, M. A., & Said, A. A. (2023). Ohmic dissipation impact on flow of Casson-Williamson fluid over a slippery surface through a porous medium. Indian Journal of Physics, 1-7.
34. Rashad, A. M., Nafe, M. A., & Eisa, D. A. (2023). Heat variation on MHD Williamson hybrid nanofluid flow with convective boundary condition and Ohmic heating in a porous material. Scientific Reports, 13(1), 6071.
35. Divya, G. P., Reddy, G. V., & Bindu, P. (2023, May). Unsteady MHD Casson and Williamson nanofluids over a permeable stretching sheet in the presence of thermal radiation and chemical reaction. In AIP Conference Proceedings (Vol. 2707, No. 1). AIP Publishing.
36. Hayat, T., Javed, T., & Abbas, Z. (2009). MHD flow of a micropolar fluid near a stagnation-point towards a non-linear stretching surface. Nonlinear Analysis: Real World Applications, 10(3), 1514-1526.
37. Mahapatra, T. R., & Gupta, A. S. (2002). Heat transfer in stagnation-point flow towards a stretching sheet. Heat and Mass transfer, 38(6), 517-521.